HHS Public Access

Author manuscript

Transl Res. Author manuscript; available in PMC 2018 October 01.

Published in final edited form as:

Transl Res. 2017 October ; 188: 10–26. doi:10.1016/j.trsl.2017.08.002.

Nanoformulated Copper/Zinc Superoxide Dismutase Exerts Differential Effects on Glucose versus Lipid Homeostasis Depending on the Diet Composition Possibly via Altered AMPK Signaling

Gopalakrishnan Natarajan[1], **Curtis Perriotte-Olson**[1], **Fatema Bhinderwala**[2,3], **Robert Powers**[2,3], **Cyrus V Desouza**[4,1], **Geoffrey A Talmon**[5], **Jiang Yuhang**[6], **Matthew C. Zimmerman**, **Alexander V Kabanov**[6], and **Viswanathan Saraswathi**[1,4,*]

[1]Department of Internal Medicine/Division of Diabetes, Endocrinology, and Metabolism, University of Nebraska Medical Center, Omaha, NE

[2]Department of Chemistry, University of Nebraska-Lincoln, NE

[3]Nebraska Center for Integrated Biomolecular Communication, University of Nebraska-Lincoln, NE

[4]VA Nebraska-Western Iowa Health Care System, Omaha, NE

[5]Department of Pathology and Microbiology, University of Nebraska Medical Center, Omaha, NE

[6]Division of Pharmacoengineering and Molecular Pharmaceutics, Eshelman School of Pharmacy, University of North Carolina at Chapel Hill, Chapel Hill, NC

Abstract

Evidence suggests that superoxide dismutase 1 (SOD1) promotes glucose versus lipid metabolism depending on the diet type. We recently reported that nanoformulated SOD1 (Nano) improved lipid metabolism without altering glucose homeostasis in high fat (HF) diet-fed mice. Here, we sought to determine the effects and potential mechanisms of Nano in modulating glucose and lipid homeostasis in mice fed a normal chow diet (CD) versus HF diet. Mice were fed a CD or a HF diet (45%) for 10 wk and injected with Nano once every two days for fifteen days. The fasting glucose level was lower (P<0.05) in CD+Nano-treated mice compared to control. Conversely, blood glucose was not altered but serum triglycerides were lower in HF+Nano-treated mice. Genes involved in fatty acid synthesis were reduced by Nano in the skeletal muscle of CD but not of HF diet-fed mice. AMPK, which promotes both glucose and lipid metabolism depending on the fuel availability, is activated by Nano in CD-fed mice. Moreover, Nano increased phosphorylation of ACC, a downstream target of AMPK, in both CD and HF diet-fed mice. Nano increased mitochondrial respiration in C2C12 myocytes in the presence of glucose or fatty acid and this

*Address correspondence to: Viswanathan Saraswathi, Research Services, VA Nebraska Western Iowa Health Care System, Omaha, NE. Ph: 402-995-3033; Fax: 402-449-0604; s.viswanathan@unmc.edu.

effect is inhibited by Compound C, an AMPK inhibitor. Our data suggest that Nano promotes glucose and lipid metabolism in CD and HF diet-fed mice, respectively, and this effect is mediated partly via AMPK signaling.

Introduction

Obesity is a worldwide problem resulting from an imbalance between energy intake and energy consumption. Superoxide dismutase (SOD) has long been known to modulate metabolism. For example, superoxide is generated from the metabolic processes that produce ATP generation from glucose and free fatty acids (FFAs). In particular, high glucose and FFAs increased superoxide generation in endothelial cells [1–3]. Therefore, proper scavenging of superoxide radicals is critical to sustain the metabolic pathways. Although SOD is essential to scavenging superoxide radicals [4, 5], the role of SOD1 in modulating glucose versus FFA metabolism which, in turn, alters systemic glucose and lipid homeostasis is still unclear.

Skeletal muscle plays a critical role in the metabolism of nutrients including glucose and FFAs [6]. In fact, skeletal muscle exhibits a high level of metabolic flexibility depending on the availability of glucose versus FFAs for ATP production [7, 8]. Of note, SOD1 transgenic mice (G86R murine SOD1 mutation) which exhibit a gain-of-function mutation, showed skeletal muscle hypermetabolism characterized by an increase in mRNA levels of genes involved in glucose and lipid metabolism [9]. These mice also exhibited a metabolic deficit as evident by reduced blood glucose, plasma lipids, and insulin and leptin levels and a reduction in adipose tissue mass. The observed metabolic deficit was reversed by a high fat (HF) diet. Another study corroborated these findings and further demonstrated that the skeletal muscle hypermetabolism was associated with an increase in the peripheral clearance of triglycerides-rich lipoproteins [10]. Together, these studies suggest that an increase in SOD1 activity promotes both glucose and FFA metabolism in skeletal muscle.

Although SOD1 regulates metabolic processes, its effects in modulating obesity-linked metabolic disorders are still unclear. The lack of a potent and highly bioavailable form of SOD1 is considered to be a major challenge in determining its effectiveness as a therapeutic agent for metabolic diseases. Research on antioxidant enzyme therapy has gained an increase in interest with the development of nanotechnology. We previously reported that nanoformulated copper/zinc SOD or SOD1 (Nano) was effective in attenuating adipose tissue inflammation in a mouse model of HF diet-induced obesity [11]. While Nano reduced plasma triglyceride (TG) levels, it did not alter systemic glucose homeostasis in these mice. Along the lines, a recent report employing the loss-of-function approach showed that CD, but not an HF diet, worsened glucose homeostasis in $SOD1^{-/-}$ mice compared to wild type mice [12]. These studies indicate that SOD1 does not alter glucose metabolism under HF diet-fed conditions. Nevertheless, the fact that $SOD1^{-/-}$ mice exhibit impaired glucose tolerance when fed a CD (relatively rich in carbohydrates) suggests that the effect of SOD1 in modulating systemic glucose versus lipid homeostasis may vary depending on which fuel is available (*i.e.* carbohydrates or fat). Based on the role of SOD1 in promoting glucose and lipid metabolism in skeletal muscle, we hypothesized that Nano is effective in improving

glucose and lipid homeostasis in CD and HF diet-fed mice, respectively, via altering skeletal muscle metabolism.

Materials and Methods

Animal

Wild type C57BL/6 mice, aged 6–8 weeks were purchased from Jackson Laboratory (Bar Harbor, ME, USA). The mice were housed in the animal facility at the Omaha VA Medical Center and cared for in accordance with the Institutional Animal Care and Use Committee (IACUC). All experimental procedures were approved by the Omaha VA IACUC. Mice were either fed a chow diet [(CD), Purina Lab Diet #5001] or a high fat (HF) diet (Research Diets Inc. #D12451) for 10 weeks. The CD consists of 29.83% protein, 56.74% carbohydrates, and 13.43% fat; whereas, the HF diet was made up of 20% protein, 35% carbohydrates and 45% fat. The HF diet was composed of 31.59%, 35.51%, and 32.91% of saturated, monounsaturated, and polyunsaturated fatty acids, respectively. After 8 weeks, the CD and HF fed mice either received HEPES buffered saline (10mM) as vehicle control or Nano (1000 units/kg body weight) via intraperitoneal injections once every two days for 15 days. A day after the last injection, the mice were subjected to fasting for five hours before being euthanized.

Nanoformulation of SOD1

Nano was prepared in 10mM HEPES buffer (pH- 7.4) as reported by Manickam *et al.*, 2012 [13]. Briefly, native bovine erythrocyte SOD1 protein (Sigma-Aldrich, St. Louis, MO, USA) was mixed with poly L-lysine-polyethylene glycol copolymer (PEG-pLL50, Alamanda Polymers™, Huntsville, AL). The SOD1 and PEG-pLL50 complex was covalently stabilized using a reducible cross-linker, 3, 3′-dithiobis (sulfosuccinimidylproprionate) (DTSSP; Thermo Fisher Scientific). The size of Nano was estimated to be ~35 nm.

Intraperitoneal Insulin Tolerance Test

Insulin tolerance test (ITT) was conducted to determine the response of mice to acute challenge with insulin. After five hours of fasting, mice were injected intraperitoneally with insulin (0.75 units/kg body weight) and blood glucose levels were measured at 0, 15, 30, 45, 60, 90, and 120 minutes using the Accu-Chek Aviva glucometer.

Intraperitoneal Glucose Tolerance Test

Glucose tolerance test (GTT) was performed to measure the ability of mice to clear injected glucose. After five hours of fasting, the mice were injected with glucose (1g/kg body weight) intraperitoneally and blood glucose levels were measured at 0, 15, 30, 60, 90, and 120 minutes using the Accu-Chek Aviva glucometer.

Intraperitoneal Pyruvate Tolerance Test

Pyruvate tolerance test (PTT) was performed to measure hepatic glucose output in response to Nano treatment. After six hours of fasting, the mice were injected with sodium pyruvate

(2g/kg body weight) intraperitoneally and blood glucose levels were measured at 0, 15, 30, 60, 90, and 120 minutes using the Accu-Chek Aviva glucometer.

Real-time PCR

Total RNA was extracted from gastrocnemius muscle samples using the TRIzol reagent (Ambion, Life Technologies). RNA was quantified using a Nano-drop spectrophotometer and 200 ng RNA was transcribed using 5x iScript reaction mix and iScript reverse transcriptase (Bio-Rad, USA). Real-time PCR was performed to determine the mRNA levels of genes regulating glucose and lipid metabolism. A ΔΔCT method was used to calculate gene expression and the values were normalized to the housekeeping gene, 18S ribosomal RNA.

Western blotting

Gastrocnemius muscle samples were lysed in a buffer containing 20mM Tris-Hcl, 150mM NaCl, 1mM EDTA, 1mM EGTA, 0.5% NP-40, 2.5mM sodium pyrophosphate, 1mM sodium orthovanadate, and protease inhibitor cocktail. Protein lysates were isolated by centrifuging samples at 12,000 rpm at 4°C for 15 minutes. Protein concentration was determined and 20 μg of protein was loaded per well. The protein bands were transferred to a PVDF membrane and immunoblotted using the following antibodies: SOD1 (Santa Cruz Biotechnology), 5′ Adenosine monophosphate-activated protein kinase alpha (AMPKα), phospho AMPKα, Acetyl-CoA carboxylase (ACC), and phospho ACC (Cell Signaling Technology). The bands were visualized using infrared (IR 700 or 800)-conjugated secondary antibodies using the Odyssey Imaging System (LI-COR Biosciences).

Histology

Gastrocnemius muscle sections (4μm) were stained with hematoxylin and eosin at the tissue sciences facility at the University of Nebraska Medical Center. These slides were reviewed by a board-certified anatomic pathologist to evaluate for significant alterations (*i.e.* myopathic changes, myositis, etc.). Images were captured at 20X magnification. Immunofluorescence analysis was performed in muscle sections to detect SOD1. Briefly, sections were de-paraffinized by three washes of xylene for three minutes each. Sections were rehydrated in a series of ethanol washes (100%, 95%, 80%, and 50% ethanol) for two minutes each followed by rinsing in water for 2 minutes. Antigen was retrieved by autoclaving the tissue sections using citrate buffer (pH6). The sections were blocked using 5% donkey serum for 1 h followed by incubation with anti-SOD1 antibody overnight. Tissue sections were washed with TBS-T buffer followed by incubation with Alexafluor 568-conjugated secondary antibody, for 1 hr. Sections were washed with TBS-T, mounted with DAPI antifade mounting solution and viewed under a Nikon Eclipse 80i fluorescence microscope (Nikon Instruments Inc. USA). Images were obtained at 20X magnification.

Thiobarbituric Acid Reactive Substances Assay

Thiobarbituric acid reactive substances (TBARs) assay was performed in gastrocnemius muscle collected from mice fed a CD or a HF diet with or without Nano treatment, using a

commercial kit (Cayman TBARs assay kit) according to the manufacturer's instructions. The absorbance was read at 530 nm.

$^{13}C_6$ Glucose Infusion for Nuclear Magnetic Resonance (NMR) Spectroscopy-based Metabolomics Analysis

Metabolomics analysis using stable isotope-labeled glucose ($^{13}C_6$ glucose) was performed using the protocol described earlier with minor modifications [14]. Mice were fed and treated with Nano as described above. At the end of the treatment period, mice were fasted for 5 h, injected with $^{13}C_6$ glucose via retro-orbital venous plexus at 1g/kg body weight, and sacrificed within 15 min. of injection. Skeletal muscle samples were collected immediately and flash frozen in liquid nitrogen for metabolomics analysis. Tissue samples were homogenized in methanol: water (1:1) mixture using the FastPrep-24 homogenizer (MP Biomedicals). Methanol was evaporated by speed vacuum centrifugation (SpeedVac R Plus, Savant). The samples were then snap frozen using liquid nitrogen and water was removed by lyophilization using a FreeZone™ (Labconco, Kansas City, MO) lyophilizer. The dried samples were then reconstituted using 550 μL of a 50 mM phosphate buffer in 100% D_2O at pH 7.2 (uncorrected) with 500 μM 3-(tetramethysilane) propionic acid-2,2,3,3-d4 (TMSP) as a chemical shift reference. The samples were centrifuged at 13,000 rpm for 5 minutes at room temperature to remove any precipitant. 500 μL of the supernatant was transferred to a 5 mm NMR tube for data acquisition. A total of 29 NMR metabolomics samples were prepared from CD-fed mice (n=7), nano-treated CD-fed mice (n=8), HF-fed mice (n=6), and nano-treated HF-fed mice (n=8).

NMR data collection and analysis

The NMR data were collected at 298K on a Bruker AVANCE III-HD 700 MHz spectrometer equipped with 5 mm quadruple resonance QCI-P cryoprobe (^{1}H, ^{13}C, ^{15}N and ^{31}P). A Bruker SampleJet sample changer with Bruker ICON-NMR software and an auto tune and match system was used to automate NMR data collection. A (2D) ^{1}H-^{13}C heteronuclear single quantum coherence (HSQC) spectra was collected for each of the 29 metabolomics samples. 2D ^{1}H-^{13}C HSQC spectra were collected at 298K with 16 dummy scans, 32 scans, and a 1.5 s relaxation delay. The 2D ^{1}H-^{13}C HSQC spectra were collected with 2K data points and a spectrum width of 4734 Hz in the direct dimension and 256 data points and a spectrum width of 18,864 Hz in the indirect dimension. The 2D ^{1}H-^{13}C HSQC spectra were processed with NMRPipe [15]. The spectra were Fourier-transformed, manually phased, zero-filled, apodized with a sine-bell window function, and baseline-corrected following solvent subtraction. All spectra were referenced to TMSP at 0 ppm. The processed spectra were then analyzed using NMRViewJ Version 8.0 [16]. The NMR spectra were manually peak-picked and the chemical shifts and peak intensities were recorded. Peak-intensities were normalized for each 2D ^{1}H-^{13}C HSQC NMR spectrum by the total peak-intensity per spectrum (*i.e.,* the total relative metabolite concentration) and by the total tissue weight per sample. Simply, the total peak intensity was summed for each individual HSQC spectrum and then the total peak intensity was scaled by the total tissue weight for the sample. Each peak within a given spectrum was then normalized to the tissue-weight scaled total peak intensity. Chemical shifts were assigned to specific metabolites using the Human Metabolomics Database (HMDB) [17], the Platform for RIKEN Metabolomics (PRIMe)

[18], and the Madison Metabolomics Consortium Database [19] A chemical shift error tolerance of 0.08 ppm and 0.25 ppm was used for ^{1}H and ^{13}C chemical shifts, respectively. A total of 23 ^{13}C-labeled metabolites derived from [$^{13}C_6$]-D-glucose were identified in the 2D ^{1}H-^{13}C HSQC NMR experiments comparing CD+Nano-treated mice to controls. Similarly, 28 metabolites were identified when the HF+Nano-treated mice were compared to controls.

Cell culture, differentiation, and treatment

The mouse skeletal muscle cell line C2C12 myoblasts were obtained from ATCC and maintained in DMEM supplemented with 15% heat inactivated FBS at 37°C with 5% CO_2. Once the cells attained 90% confluency, the growth media was replaced by differentiation medium containing 2% equine donor serum with insulin (100μM/mL) to differentiate the cells into myotubes. The differentiation protocol was slightly modified [20, 21] and experiments were performed after 7 days of differentiation. Briefly, the myocytes were treated with native SOD or Nano at 200 U/mL for 6 h. The cells were rinsed in PBS and incubated in fresh medium overnight. Cell lysates were collected the following day and analyzed for SOD1 protein content by western blot analysis. Markers of AMPK signaling were also determined.

Oxygen consumption rate

The mitochondrial oxygen consumption rate (OCR) was measured using a Seahorse XF^{e}24 Extracellular Flux Analyzer (Seahorse Bioscience) according to the manufacturer's instructions. C2C12 myoblasts were cultured in Dulbecco's Modified Eagle's Medium supplemented with 20% FBS, and 1% penicillin-streptomycin on a XF assay plate at a density of 40,000 cells per well. After 24 h, the cells were treated with Nano for 6 h, washed with DMEM, and incubated overnight. The cells were washed with XF assay medium (Seahorse Bioscience). The glucose concentration in the XF assay medium was 2.5 mM (low glucose medium). Pyruvate was not added to the assay medium since we wanted to study the role of Nano in modulating glucose-induced changes in OCR. Cells were supplemented with 25 mM glucose (high glucose) in separate wells. To study the role of Nano in modulating fatty acid-induced changes in OCR, Nano pre-treated cells were treated with oleic acid complexed to BSA. The fatty acid:BSA complex was prepared as we described previously [22]. Briefly, after Nano pre-treatment, the cells were treated with oleic acid using the XF assay medium. Culture plates were incubated in a non-CO_2 incubator for 1 h at 37°C. A calibration sensor cartridge and culture plate containing XF Calibrant (Seahorse Bioscience), previously incubated at 37°C without CO_2 for 24 h was loaded into an XF^{e}24 analyzer. After calibration/equilibration the culture plate was loaded, followed by injection of reagents such as oligomycin (1 μM), FCCP (1 μM) and rotenone/antimycin (1 μM) according to priority. Oxygen consumption rate (OCR) was automatically calculated and recorded by the Seahorse XF24 software. Basal respiration [(last rate measurement before oligomycin injection) – Non-mitochondrial respiration (minimum rate measurement after rotenone/antimycin injection)], Maximal respiration [(maximum rate measurement after FCCP injection) – Non-mitochondrial respiration (minimum rate measurement after rotenone/antimycin injection)]; ATP production [(last rate measurement before oligomycin injection) – (minimum rate measurement after oligomycin injection)] and spare respiratory

capacity (%) [(maximal respiration)/(basal respiration) x 100] were calculated as per the manufacturer's instructions. In some experiments, cells were treated with Nano in the presence or absence of Compound C, an AMPK inhibitor, followed by treatment with glucose or oleic acid. Values were not normalized to the total protein concentration since the cell monolayer was intact and there were no signs of dead cells.

Statistical analyses

Values are expressed as mean ± SEM. Statistical analysis was performed by an unpaired two-tailed Student's *t* test. The Benjamini-Hochberg multiple hypothesis test correction was applied to the metabolomics data and Benjamini-Hochberg corrected *P* values are reported [23]. The Graph-Pad prism software was used for statistical analysis and a statistical probability of $P < 0.05$ was considered significant.

Results

Effect of Nano on metabolic variables in mice

Mice were grouped into: 1) Control-CD; 2) CD+Nano; 3) Control-HF, and 4) HF+Nano. Mice fed a HF diet showed an increase in body weight, body weight gain, and fat mass compared to CD groups [11]. The Nano treatment did not alter any of these parameters in the CD (data not shown) or the HF fed groups [11]. Interestingly, the fasting blood glucose level was significantly lower in the CD+Nano group ($P<0.05$) compared to CD controls (Fig. 1A), but the blood glucose levels were not altered in HF+Nano-treated mice (Fig. 1F) as we reported previously [11]. Serum total cholesterol levels were not altered between control and Nano-treated mice fed either CD or HF diet (Fig. 1B&G). While the serum triglyceride level was not altered by Nano in CD-fed mice, we noted significantly lower levels of triglycerides in HF+Nano-treated mice compared to HF controls ($P<0.05$) (Fig. 1C&H). Taken together, these data indicate that Nano improves glucose and lipid metabolism in CD and HF diet-fed mice, respectively. Serum insulin levels were not significantly altered but did show an increasing trend in both CD and HF-fed mice upon Nano treatment (Fig. 1D&I). Similarly, HOMA-IR, a measure of insulin resistance, did not significantly change after Nano treatment but showed a trend towards an increase in HF+Nano-treated mice compared to HF controls (Fig. 1E&J).

Effect of Nano on Insulin sensitivity and Glucose Homeostasis

We recently showed that Nano did not alter systemic glucose homeostasis in mice fed a HF diet [11]. In the current study, we performed ITT and GTT in CD and CD+Nano-treated mice to determine the role of Nano in regulating systemic glucose handling. The ITT revealed no difference between CD-control and CD+Nano groups upon an acute challenge with insulin (Fig. 2A). Accordingly, the area under the curve (AUC) of the blood glucose during ITT was not altered significantly in Nano-treated mice compared to CD controls (Fig. 2B), indicating that the systemic insulin sensitivity was not altered in these mice. GTT showed that the ability of mice to clear glucose levels after an acute glucose injection did not vary between groups (Fig. 2C&D), which indicates that the acute insulin secretion by the pancreas upon glucose challenge is not altered by Nano. Since the fasting blood glucose was lower in CD+Nano-treated mice, we next performed the PTT to determine if the reduction in

fasting blood glucose was due to reduced hepatic gluconeogenesis. Our data showed that hepatic glucose output is not altered between CD and CD+Nano-treated mice (Fig. 2E&F). An analysis of gluconeogenic markers in liver showed no difference between control and Nano-treated mice (Fig. 2G). Overall, these data show that Nano reduces fasting blood glucose levels without altering systemic insulin sensitivity and hepatic gluconeogenesis in mice fed a CD.

Nano delivers SOD1 to skeletal muscle

Previous studies in SOD1 mutant mice with a gain-of-function mutation showed that skeletal muscle exhibits hypermetabolism [24, 25]. Therefore, we proceeded to determine the role of Nano in modulating glucose versus lipid metabolism in the skeletal muscle of CD or HF fed mice. First, we performed the H&E staining to determine if any histological changes occurred in Nano-treated mice on a CD or HF diet relative to controls. Microscopic examination of the muscle section did not reveal any notable changes. Specifically, there was no evidence of atrophy or myofibril loss. Markers of inflammation, vasculitis, and intravascular thrombi were absent. Myofibrils did not reveal any abnormal distribution of sarcoplasmic proteins, and striations were intact in longitudinal sections (Fig. 3A–D). We next determined whether Nano treatment increases the accumulation of SOD1 in skeletal muscle. Immunofluorescence analysis showed a remarkable increase in SOD1 protein in CD +Nano-treated mice compared to CD control (Fig. 3E&F). However, muscle SOD1 content was not significantly altered in the HF+Nano group compared to HF controls (Fig. 3G&H). Western blot analysis further confirmed that the SOD1 protein was significantly higher in CD+Nano-treated mice compared to CD controls ($P<0.05$) (Fig. 3I); whereas, the muscle SOD1 protein was not significantly altered by Nano in HF-fed mice (Fig. 3J).

Nano is effective in reducing skeletal muscle oxidative stress in CD-fed mice

TBARs generated by lipid peroxidation are considered to be a marker of oxidative stress. We measured TBARs levels in skeletal muscle and noted that the levels of these lipid peroxidation products are significantly lower in muscles derived from CD+Nano-treated mice compared to CD controls (Fig. 4A) ($P<0.05$). However, Nano did not alter the level of TBARs in HF fed mice (Fig. 4B).

Modulatory effect of Nano on muscle expression of genes involved in glucose and lipid metabolism

Because fasting blood glucose was lower in CD+Nano-treated mice, we next determined the mRNA levels of genes involved in glucose metabolism in muscle. We did not see a significant difference in the mRNA levels of *Glut4*, *Glut1*, hexokinase 2 (*Hx-II*), and *Pfkfb3* in skeletal muscle of Nano-treated mice compared to CD controls (Fig. 5A). *Glut-1* expression showed a trend towards a decrease in HF+Nano-treated mice compared to HF controls (Fig. 5B). Regarding genes altering fatty acid metabolism, we noted distinct effects with Nano treatment in CD versus HF diet-fed conditions. For example, markers of fatty acid oxidation including *Acox1* and *Cpt2* were significantly lower in CD+Nano-treated mice compared to controls (Fig. 5C). Conversely, *Acox1* expression showed a marginal increase ($P<0.06$) in HF+Nano-treated mice compared to HF controls (Fig. 5D). Markers of fatty acid synthesis including *Pcx* and *Srebp1f* were significantly lower in CD+Nano-treated mice;

whereas, the expression of these genes were not significantly altered in HF+Nano-treated mice compared to controls (Fig. 5E&F). Taken together, these data indicate that under CD-fed conditions, where the supply of dietary fatty acids is low, Nano impairs *de novo* lipogenesis and fatty acid oxidation in skeletal muscle. While Nano does not change the expression of lipogenic markers, it increases markers of fatty acid oxidation to some extent in HF diet-fed mice.

Nano increases muscle AMPK signaling in mice fed a CD or a HF diet

Next, we sought to determine the mechanisms by which Nano alters glucose and lipid homeostasis. To this end, we investigated the impact Nano has on increasing AMPK signaling, which promotes both glucose and fatty acid metabolism [26, 27]. Western blot analysis revealed a significant increase in both total ($P<0.01$) and phosphorylated forms of AMPK ($P<0.05$) in Nano-treated mice compared to controls on a CD (Fig. 6A–C). Moreover, the level of phosphorylated ACC, a downstream target of AMPK signaling, was significantly higher in CD+Nano-treated mice compared to CD controls (Fig. 6A&D). These data indicate that an increase in muscle AMPK signaling may play a role in mediating the effect of Nano in reducing fasting blood glucose levels. Regarding the role of Nano in promoting AMPK signaling on a HF diet, phospho AMPK was not altered in HF+Nano-treated mice compared to HF controls (Fig. 6F–H). However, we noted a significant increase in both total ($P<0.05$) and phosphorylated ACC ($P<0.001$) levels in Nano-treated mice on a HF diet (Fig. 6F, I&J). Since phosphorylation of ACC at Ser79 residue is catalyzed by AMPK [28], these data suggest that Nano has the potential to also increase muscle AMPK signaling in HF diet-fed mice.

Effect of Nano on the enrichment of ^{13}C in muscle

Although fasting blood glucose was reduced and AMPK signaling was increased by Nano treatment in CD-fed mice, the mRNA levels of genes involved in glucose uptake and metabolism were unaltered in muscle. Therefore, we performed a metabolomics analysis using the stable isotope-labeled [$^{13}C_6$]-D-glucose to determine the impact of Nano treatment on glucose metabolism in skeletal muscle. The total ^{13}C enrichment in muscle (Fig. 7A) and in glucose and glucose-6-phosphate (Fig. 7B) appeared to increase in CD+Nano-treated mice compared to CD controls, but the changes were not statistically confirmed ($P > 0.1$). Interestingly, the ^{13}C enrichment in glucuronic acid, a glucose metabolite, may be slightly higher in CD+Nano-treated mice compared to CD controls (Fig. 7B). While the changes in glucuronic acid were significant based solely on a pairwise comparison ($P=0.04$), it fell below statistical significance after correcting for a multiple hypothesis test ($P=0.07$). Conversely, ^{13}C enrichment was not altered at all in muscle of HF+Nano-treated mice compared to HF controls (Fig. 7C&D). Taken together, these data suggest that Nano may minimally increase glucose uptake and metabolism in skeletal muscle in CD-fed mice but not in HF fed mice. However, further studies with longer treatment with ^{13}C-labeled glucose are needed to confirm this notion.

Effect of Nano on the delivery of SOD1 to myocytes and the activation of AMPK signaling

We previously reported that Nano preferentially delivers SOD1 to endothelial cells compared to native unmodified SOD1 [29]. To determine whether Nano effectively delivers

SOD1 to myocytes, we performed *in vitro* studies in cultured C2C12 myocytes. We differentiated C2C12 myoblasts into myocytes (Fig. 8A&B) by culturing myoblasts in media containing horse serum for 7 days [20]. We then treated the mature myocytes with native- or nano-SOD. As shown in Fig. 8C&D, Nano treatment led to a profound increase in SOD1 protein in myocytes. We noted a significant 2-fold increase in SOD1 protein levels in myocytes treated with Nano ($P<0.001$) compared to control whereas native-SOD did not increase the cellular levels of SOD1. We next analyzed markers of AMPK signaling in these cells to determine the direct effects of SOD1 in modulating AMPK signaling. Interestingly, we noted a trend towards an increase and a significant increase in phospho AMPK and phospho ACC, respectively, in cells treated with Nano compared to control whereas AMPK signaling was unaltered in cells treated with native-SOD (Fig 8C, E–H). Together, these data provide evidence SOD1 may alter metabolic processes by modulating muscle AMPK signaling.

Effect of Nano in modulating mitochondrial respiration in the presence of glucose or fatty acid

Since AMPK and/or ACC phosphorylation were significantly increased in Nano-treated C2C12 cells, we next investigated the impact of Nano in altering mitochondrial respiration in the presence of glucose or fatty acid. We used both low and high glucose media to determine the effect of Nano on mitochondrial respiration. As previously reported [30], the presence of high glucose actually reduced mitochondrial respiration as evident from a reduction in basal respiration, maximal respiration, ATP production, and spare respiratory capacity (Fig. 9A). However, Nano was able to increase the maximal respiration and spare respiratory capacity in cells treated with low or high glucose medium suggesting the ability of Nano in promoting glucose metabolism under conditions of high energy demand (Fig. 9A). ATP production was not significantly altered by Nano treatment. To determine whether inhibition of AMPK activity inhibits the effects of Nano on mitochondrial respiration, we pretreated cells with Compound C, an AMPK inhibitor at 5 μM concentration followed by treatment with Nano and 2.5 mM glucose. Compound C was effective in reducing basal and maximal respiration as well as ATP production indicating that AMPK does play a role in mediating the effects of Nano on glucose metabolism (Fig. 9B). It should be noted that the spare respiratory capacity is higher in Compound C treated cells. This can be attributed to the low basal and maximal respiration in this group.

We next determined the effect of Nano in modulating mitochondrial respiration in the presence of the free fatty acid, oleic acid (OA). As shown in Fig. 9C, the basal respiration trended towards an increase in OA-treated cells whereas it was significantly increased in Nano+OA-treated cells ($P<0.01$). The maximal respiration was significantly increased in Nano+OA-treated cells compared to control and OA-treated cells. Interestingly, ATP production was lower in OA-treated cells compared to control but Nano pretreatment led to an increase in ATP production. Similarly, the spare respiratory capacity was significantly reduced in OA-treated cells whereas we noted a significant increase in this variable in Nano +OA-treated cells compared to control and OA-treated cells. Together, these data provide evidence that Nano increases mitochondrial respiration in the presence of fatty acids. In addition, Nano+OA in the presence of Compound C exhibited a reduction in basal and

maximal respiration and ATP production indicating that AMPK has a role in mediating the effect of Nano on fatty acid metabolism (Fig. 9D).

Discussion

The role of SOD1 in altering glucose versus free fatty acid metabolism remains unclear. Using a novel nanoformulated SOD1 we have demonstrated that SOD1 promotes glucose and lipid metabolism in a diet-dependent manner (*i.e.* CD versus HF). In particular, we have provided evidence that Nano lowers blood glucose and serum triglyceride levels in CD and HF diet-fed conditions, respectively. Our data showed that Nano was effective in delivering SOD1 to skeletal muscle and in reducing markers of oxidative stress, in particular, TBARs. As for the role of Nano on muscle metabolic markers, we showed that markers of lipogenesis were downregulated by Nano in CD but not in HF fed mice. Furthermore, we have provided evidence that Nano increased AMPK and/or ACC phosphorylation in CD and HF fed mice. Further, we have demonstrated that ACC-Ser^{79} phosphorylation is higher in C2C12 cells treated with Nano, indicating increased AMPK signaling. Moreover, we have shown that inhibition of AMPK signaling using Compound C inhibited Nano+glucose and Nano+OA–mediated increase in mitochondrial respiration. Collectively, our data suggest that SOD1 can differentially modulate glucose and lipid metabolism based on specific fuel availability and this effect is mediated at least in part, via activation of the energy sensor, AMPK, in skeletal muscle.

We and others have shown that SOD1 has a critical role in regulating lipid homeostasis [11, 31]. For example, we previously reported that delivering SOD1 as Nano reduced plasma and liver triglycerides [11]. Similarly, Pires *et al.* showed that MnTBAP, a SOD mimetic, reduced plasma FFAs in mice fed a HF diet [31]. However, the systemic glucose homeostasis was not altered by SOD therapy in either of these studies, raising questions regarding the role of SOD1 in altering glucose metabolism. Interestingly, a recent study showed that SOD1$^{-/-}$ mice exhibited an impaired glucose homeostasis when provided a normal CD [12]. However, an HF diet did not result in glucose intolerance in SOD1$^{-/-}$ mice relative to WT mice. Together, these studies indicate that SOD1 has the propensity to promote both glucose and lipid metabolism, and this effect is dependent on the diet composition.

Although muscle expression of glucoregulatory genes was not altered, we noted a decrease in fasting blood glucose in Nano-treated mice on a CD, indicating increased glucose metabolism. Since the activities of enzymes involved in glucose metabolism are also regulated by allosteric mechanisms [32–34], it is also possible that the reduction in glucose levels are due to increased activities of these enzymes and this possibility requires further investigation. As for the role of SOD1 in increasing glucose metabolism in muscle, our metabolomics data show that the uptake/metabolism of ^{13}C glucose showed only a trend towards an increase in the muscle of CD+Nano-treated mice. However, it should be pointed out that the mice were euthanized 15 min after administering ^{13}C-labeled glucose and therefore a longer treatment time with labeled glucose may provide a better understanding on the role of nanoSOD in modulating muscle glucose uptake *in vivo*. While our current *in vivo* data do not fully support the role of muscle in mediating the glucose-lowering effect of

Nano, our studies in cultured C2C12 cells showed that Nano increased cellular respiration upon treatment with glucose or fatty acid. Nonetheless, in the absence of changes in ITT, GTT, and PTT, it is unclear as to the potential mechanisms involved in mediating the glucose-lowering effect of Nano in CD-fed mice.

We noted a reduction in serum and liver triglycerides [11] in Nano-treated mice compared to control mice on an HF diet, indicating improved lipid handling. This is further supported by our observation that Nano showed a marginal increase in the mRNA level of *Acox1*, a gene involved in fatty acid oxidation. Conversely, the expression of *Acox1* and *Cpt2* was lower in CD+Nano-treated mice compared to CD controls indicating that fatty acid oxidation was lower in CD+Nano-treated mice compared to CD controls. Moreover, genes involved in fatty acid synthesis were down-regulated in CD+Nano-treated mice. Our data on lipid metabolism-related genes actually support our notion that in the presence of excess carbohydrate in the diet, glucose but not lipid metabolism is increased in the skeletal muscle of CD+Nano-treated mice. However, it is unclear as to why the plasma TG levels are not altered despite changes in mRNA levels of genes involved in lipogenesis and lipid oxidation. One plausible explanation may be that the decrease in lipogenesis is balanced by a corresponding decrease in fatty acid oxidation which ultimately leads to no changes in systemic TG levels in CD+Nano-treated mice. It should also be pointed out that the CD and HF groups exhibit different degree of adiposity and therefore, the presence or absence of obesity in these mice may have a role in differentially altering glucose versus fatty acid metabolism upon Nano treatment. However, *in vitro* studies in C2C12 cells on mitochondrial respiration showed that basal and/or maximum respiration and spare respiratory capacity were increased significantly in glucose or oleic acid-treated cells in the presence of Nano indicating that Nano can effectively metabolize glucose or fatty acids depending on the availability of substrates.

The notion that SOD1 differentially promotes glucose versus lipid metabolism depending on the diet type is supported by the observation that Nano in the current study increases AMPK and phospho AMPK and/or its downstream target ACC and phospho ACC in skeletal muscle of CD and HF diet-fed mice. AMPK is an energy sensor, which exhibits a high degree of metabolic flexibility. AMPK activation is known to regulate both glucose and lipid metabolism depending on the fuel availability [35, 36]. Of note, AICAR, an AMPK agonist, and metformin are known to activate AMPK in skeletal muscle and improve glucose uptake and metabolism [37, 38]. Thus, a decrease in fasting blood glucose in Nano-treated mice on a CD may be due to an increase in muscle AMPK signaling and a corresponding increase in glucose metabolism in skeletal muscle. While further studies are needed to confirm this possibility *in vivo*, studies in C2C12 cells showed that Nano increased cellular respiration upon glucose treatment which was attenuated by the AMPK inhibitor, indicating the ability of Nano in promoting glucose metabolism and the role of AMPK in mediating this.

Of note, in addition to glucose metabolism, the activation of AMPK/ACC axis also promotes fatty acid oxidation and reduces lipogenesis. For example, phosphorylation of ACC by AMPK inhibits ACC activity thereby attenuating fatty acid synthesis and increasing fatty acid oxidation [39]. Although AMPK phosphorylation was not altered by Nano treatment in HF-fed mice, the phosphorylation of ACC at Ser^{79}, a downstream target of AMPK, was

significantly higher indicating an increased AMPK activation. In fact, AMPK is the main kinase regulator of ACC and is the upstream kinase for ACC Ser^{79} phosphorylation [28, 40]. The effectiveness of Nano in promoting AMPK signaling is further supported by the observation that inhibition of AMPK activity with Compound C attenuated the Nano-induced increase in mitochondrial respiration in glucose or fatty acid-treated myocytes.

It is important to note that Nano treatment led to an increase in SOD1 protein levels and a decrease in oxidative stress in muscle of CD-fed mice but not in HF-fed mice. In fact, we previously reported that Nano was effective in reducing adipose tissue inflammation, but this was not associated with an increase in SOD1 protein levels or a reduction in markers of oxidative stress in adipose tissue [11]. It is unclear as to why Nano treatment increases SOD1 protein levels in the skeletal muscle of CD-fed but not in HF-fed mice. An efficient uptake of nanoparticles by macrophages [41] and a rapid clearance in HF-fed mice may be one plausible explanation. In fact, obesity is associated with systemic monocyte activation and an increase in skeletal muscle macrophage content [42, 43]. It has also been previously shown that nanoparticles are easily taken up by monocytes/macrophages [44, 45]. Thus, it is likely that Nano is taken up by these monocytes/macrophages and cleared from the system at a faster rate in HF-fed mice compared to CD-fed mice. Moreover, we euthanized mice 24 h post-injection and therefore, a time course study in HF diet-fed mice after Nano injection would be helpful to better determine its effectiveness in increasing SOD1 delivery in muscle and its antioxidant potential in this experimental condition. Nevertheless, Nano treatment resulted in changes in muscle AMPK/ACC phosphorylation and serum triglycerides, indicating that it was indeed able to exert the biological effects leading to an improved lipid handling. Furthermore, our *in vitro* studies in cultured myotubes provide evidence that Nano effectively delivered SOD1 to myocytes which, in turn, exerted direct effects on AMPK signaling.

Clinically, our study provides proof-of-concept data for considering Nano to ameliorate lipid disorders in obesity. Our findings provide important information regarding the potential of SOD1 in modulating glucose and lipid metabolism depending on the substrate availability. This is especially important for patients with amyotrophic lateral sclerosis (ALS) who exhibit SOD1 gain-of-function. Intriguingly, hypermetabolism is one of the characteristics of ALS. Of note, a high energy diet improved the survival of these patients [46, 47]. However, it is still unclear what SOD1-dependent metabolic functions are altering the energy balance in these ALS patients. Accordingly, our study provides evidence that SOD1 promotes both glucose and lipid metabolism and suggest that this effect may be mediated through muscle AMPK signaling. Furthermore, our results suggest that the energy deficient state seen in ALS patients may be overcome to some extent by a HF diet which, by nature, provides more energy than a normal diet. Our study demonstrates that SOD1 is effective in promoting glucose and lipid metabolism in muscle and this effect depends on the diet type, in particular, the availability of carbohydrates or fat as energy source. The differential effects of Nano in modulating glucose versus lipid metabolism are mediated in part, via AMPK/ACC signaling.

Acknowledgments

Funding. The work was supported by the NIH-Nebraska Center for Nanomedicine COBRE Grant (2P20GM103480) and Mary and Dick Holland Regenerative Medicine Program Pilot Project. AVK and JY acknowledge the support of *The Carolina Partnership*, a strategic partnership between the UNC Eshelman School of Pharmacy and the University Cancer Research Fund through the Lineberger Comprehensive Cancer Center. RP is supported by the Nebraska Center for Integrated Biomolecular Communication Systems Biology Core (NIH-NIGMS P20-GM113126) and the Redox Biology Center (NIH/NIGMS P30 GM103335).

This paper is the result of work conducted with the resources and the facilities at the VA-Nebraska Western Iowa Health Care System, Omaha. All authors have read the journal's authorship agreement and policy on disclosure of potential conflicts of interest. All authors were involved in the review of the manuscript and had final approval of the submitted version. AVK is the co-inventor of the nanozyme technology at UNMC (Patent number: WO2008141155A1). The technology and products have been exclusively out-licensed to NeuroNano Pharma, a start-up company located in Chapel Hill, NC. AVK is a co-founder, shareholder and director of this company.

Abbreviations

ACC	Acetyl-coA carboxylase
ACOX1	Acyl-CoA oxidase1
AMPK	AMP-activated protein kinase
DTSSP	3,3′-Dithiobis (sulfosuccinimidylpropionate)
FABP1	Fatty acid binding protein 1
FASN	Fatty acid synthase
Glut1	Glucose transporter1
Glut4	Glucose transporter type 4
GTT	Glucose tolerance test
HK2	Hexokinase 2
ITT	Insulin tolerance test
LPL	Lipoprotein lipase
OCR	Oxygen consumption rate
PCK2	Phosphoenolpyruvate carboxykinase 2
PCX	Pyruvate carboxylase
PEG	Polyethylene glycol
pLL	Poly-L-lysine
PTT	Pyruvate tolerance test
SOD1	Superoxide dismutase 1
SREBP1	Sterol regulatory element-binding protein 1

TBARs Thiobarbituric acid reactive substances

References

1. Cosentino F, Hishikawa K, Katusic ZS, Luscher TF. High glucose increases nitric oxide synthase expression and superoxide anion generation in human aortic endothelial cells. Circulation. 1997; 96:25–8. [PubMed: 9236411]
2. Du X, Edelstein D, Obici S, et al. Insulin resistance reduces arterial prostacyclin synthase and eNOS activities by increasing endothelial fatty acid oxidation. J Clin Invest. 2006; 116:1071–80. [PubMed: 16528409]
3. Paneni F, Costantino S, Cosentino F. Role of oxidative stress in endothelial insulin resistance. World J Diabetes. 2015; 6:326–32. [PubMed: 25789114]
4. Fukai T, Ushio-Fukai M. Superoxide dismutases: role in redox signaling, vascular function, and diseases. Antioxid Redox Signal. 2011; 15:1583–606. [PubMed: 21473702]
5. Finkel T, Holbrook NJ. Oxidants, oxidative stress and the biology of ageing. Nature. 2000; 408:239–47. [PubMed: 11089981]
6. Wolfe RR. The underappreciated role of muscle in health and disease. Am J Clin Nutr. 2006; 84:475–82. [PubMed: 16960159]
7. Turner N, Cooney GJ, Kraegen EW, Bruce CR. Fatty acid metabolism, energy expenditure and insulin resistance in muscle. J Endocrinol. 2014; 220:T61–79. [PubMed: 24323910]
8. Zhang S, Hulver MW, McMillan RP, Cline MA, Gilbert ER. The pivotal role of pyruvate dehydrogenase kinases in metabolic flexibility. Nutr Metab (Lond). 2014; 11:10. [PubMed: 24520982]
9. Dupuis L, Oudart H, Rene F, Gonzalez de Aguilar JL, Loeffler JP. Evidence for defective energy homeostasis in amyotrophic lateral sclerosis: benefit of a high-energy diet in a transgenic mouse model. Proc Natl Acad Sci U S A. 2004; 101:11159–64. [PubMed: 15263088]
10. Fergani A, Oudart H, Gonzalez De Aguilar JL, et al. Increased peripheral lipid clearance in an animal model of amyotrophic lateral sclerosis. J Lipid Res. 2007; 48:1571–80. [PubMed: 17438338]
11. Perriotte-Olson C, Adi N, Manickam DS, et al. Nanoformulated copper/zinc superoxide dismutase reduces adipose inflammation in obesity. Obesity (Silver Spring). 2016; 24:148–56. [PubMed: 26612356]
12. Muscogiuri G, Salmon AB, Aguayo-Mazzucato C, et al. Genetic disruption of SOD1 gene causes glucose intolerance and impairs beta-cell function. Diabetes. 2013; 62:4201–7. [PubMed: 24009256]
13. Manickam DS, Brynskikh AM, Kopanic JL, et al. Well-defined cross-linked antioxidant nanozymes for treatment of ischemic brain injury. J Control Release. 2012; 162:636–45. [PubMed: 22902590]
14. Fan TW, Lane AN, Higashi RM, Yan J. Stable isotope resolved metabolomics of lung cancer in a SCID mouse model. Metabolomics. 2011; 7:257–69. [PubMed: 21666826]
15. Delaglio F, Grzesiek S, Vuister GW, et al. NMRPipe: a multidimensional spectral processing system based on UNIX pipes. J Biomol NMR. 1995; 6:277–93. [PubMed: 8520220]
16. Johnson BA. Using NMRView to visualize and analyze the NMR spectra of macromolecules. Methods Mol Biol. 2004; 278:313–52. [PubMed: 15318002]
17. Wishart DS, Jewison T, Guo AC, et al. HMDB 3.0--The Human Metabolome Database in 2013. Nucleic Acids Res. 2013; 41:D801–7. [PubMed: 23161693]
18. Akiyama K, Chikayama E, Yuasa H, et al. PRIMe: a Web site that assembles tools for metabolomics and transcriptomics. In Silico Biol. 2008; 8:339–45. [PubMed: 19032166]
19. Cui Q, Lewis IA, Hegeman AD, et al. Metabolite identification via the Madison Metabolomics Consortium Database. Nat Biotechnol. 2008; 26:162–4. [PubMed: 18259166]
20. Tannu NS, Rao VK, Chaudhary RM, et al. Comparative proteomes of the proliferating C(2)C(12) myoblasts and fully differentiated myotubes reveal the complexity of the skeletal muscle differentiation program. Mol Cell Proteomics. 2004; 3:1065–82. [PubMed: 15286212]

21. Casas-Delucchi CS, Brero A, Rahn HP, et al. Histone acetylation controls the inactive X chromosome replication dynamics. Nat Commun. 2011; 2:222. [PubMed: 21364561]
22. Saraswathi V, Hasty AH. Inhibition of long-chain acyl coenzyme A synthetases during fatty acid loading induces lipotoxicity in macrophages. Arterioscler Thromb Vasc Biol. 2009; 29:1937–43. [PubMed: 19679826]
23. Benjamini Y, Hochberg Y. Controlling the false discovery rate: a practical and powerful approach to multiple testing. J R Statist B. 1995; 57:289–300.
24. Dupuis L, Gonzalez de Aguilar JL, Echaniz-Laguna A, et al. Muscle mitochondrial uncoupling dismantles neuromuscular junction and triggers distal degeneration of motor neurons. PLoS One. 2009; 4:e5390. [PubMed: 19404401]
25. Dupuis L, di Scala F, Rene F, et al. Up-regulation of mitochondrial uncoupling protein 3 reveals an early muscular metabolic defect in amyotrophic lateral sclerosis. FASEB J. 2003; 17:2091–3. [PubMed: 14500553]
26. Srivastava RA, Pinkosky SL, Filippov S, et al. AMP-activated protein kinase: an emerging drug target to regulate imbalances in lipid and carbohydrate metabolism to treat cardio-metabolic diseases. J Lipid Res. 2012; 53:2490–514. [PubMed: 22798688]
27. Watt MJ, Steinberg GR, Chen ZP, Kemp BE, Febbraio MA. Fatty acids stimulate AMP-activated protein kinase and enhance fatty acid oxidation in L6 myotubes. J Physiol. 2006; 574:139–47. [PubMed: 16644805]
28. Ha J, Daniel S, Broyles SS, Kim KH. Critical phosphorylation sites for acetyl-CoA carboxylase activity. J Biol Chem. 1994; 269:22162–8. [PubMed: 7915280]
29. Saraswathi V, Ganesan M, Perriotte-Olson C, et al. Nanoformulated copper/zinc superoxide dismutase attenuates vascular cell activation and aortic inflammation in obesity. Biochem Biophys Res Commun. 2016; 469:495–500. [PubMed: 26692492]
30. Elkalaf M, Andel M, Trnka J. Low glucose but not galactose enhances oxidative mitochondrial metabolism in C2C12 myoblasts and myotubes. PLoS One. 2013; 8:e70772. [PubMed: 23940640]
31. Pires KM, Ilkun O, Valente M, Boudina S. Treatment with a SOD mimetic reduces visceral adiposity, adipocyte death, and adipose tissue inflammation in high fat-fed mice. Obesity (Silver Spring). 2014; 22:178–87. [PubMed: 23526686]
32. Virkamaki A, Yki-Jarvinen H. Allosteric regulation of glycogen synthase and hexokinase by glucosamine-6-phosphate during glucosamine-induced insulin resistance in skeletal muscle and heart. Diabetes. 1999; 48:1101–7. [PubMed: 10331416]
33. Schoneberg T, Kloos M, Bruser A, Kirchberger J, Strater N. Structure and allosteric regulation of eukaryotic 6-phosphofructokinases. Biol Chem. 2013; 394:977–93. [PubMed: 23729568]
34. Donovan KA, Zhu S, Liuni P, et al. Conformational Dynamics and Allostery in Pyruvate Kinase. J Biol Chem. 2016; 291:9244–56. [PubMed: 26879751]
35. Hardie DG, Scott JW, Pan DA, Hudson ER. Management of cellular energy by the AMP-activated protein kinase system. FEBS Lett. 2003; 546:113–20. [PubMed: 12829246]
36. Long YC, Zierath JR. AMP-activated protein kinase signaling in metabolic regulation. J Clin Invest. 2006; 116:1776–83. [PubMed: 16823475]
37. Bergeron R, Previs SF, Cline GW, et al. Effect of 5-aminoimidazole-4-carboxamide-1-beta-D-ribofuranoside infusion on in vivo glucose and lipid metabolism in lean and obese Zucker rats. Diabetes. 2001; 50:1076–82. [PubMed: 11334411]
38. Koistinen HA, Galuska D, Chibalin AV, et al. 5-amino-imidazole carboxamide riboside increases glucose transport and cell-surface GLUT4 content in skeletal muscle from subjects with type 2 diabetes. Diabetes. 2003; 52:1066–72. [PubMed: 12716734]
39. Fediuc S, Gaidhu MP, Ceddia RB. Regulation of AMP-activated protein kinase and acetyl-CoA carboxylase phosphorylation by palmitate in skeletal muscle cells. J Lipid Res. 2006; 47:412–20. [PubMed: 16304351]
40. Park SH, Gammon SR, Knippers JD, et al. Phosphorylation-activity relationships of AMPK and acetyl-CoA carboxylase in muscle. J Appl Physiol (1985). 2002; 92:2475–82. [PubMed: 12015362]
41. Di Mascolo D, CJL, Aryal S, et al. Rosiglitazone-loaded nanospheres for modulating macrophage-specific inflammation in obesity. J Control Release. 2013; 170:460–8. [PubMed: 23791978]

42. Khan IM, Pokharel Y, Dadu RT, et al. Postprandial Monocyte Activation in Individuals With Metabolic Syndrome. J Clin Endocrinol Metab. 2016; 101:4195–204. [PubMed: 27575945]

43. Pincu Y, Linden MA, Zou K, Baynard T, Boppart MD. The effects of high fat diet and moderate exercise on TGFbeta1 and collagen deposition in mouse skeletal muscle. Cytokine. 2015; 73:23–9. [PubMed: 25689619]

44. Corot C, Robert P, Idee JM, Port M. Recent advances in iron oxide nanocrystal technology for medical imaging. Adv Drug Deliv Rev. 2006; 58:1471–504. [PubMed: 17116343]

45. Luciani N, Wilhelm C, Gazeau F. The role of cell-released microvesicles in the intercellular transfer of magnetic nanoparticles in the monocyte/macrophage system. Biomaterials. 2010; 31:7061–9. [PubMed: 20619790]

46. Genton L, Viatte V, Janssens JP, Heritier AC, Pichard C. Nutritional state, energy intakes and energy expenditure of amyotrophic lateral sclerosis (ALS) patients. Clin Nutr. 2011; 30:553–9. [PubMed: 21798636]

47. Wills AM, Hubbard J, Macklin EA, et al. Hypercaloric enteral nutrition in patients with amyotrophic lateral sclerosis: a randomised, double-blind, placebo-controlled phase 2 trial. Lancet. 2014; 383:2065–72. [PubMed: 24582471]

Background

The role of SOD1 in regulating glucose and lipid metabolism remains unclear. We previously reported that nanoformulated copper/zinc SOD (Nano) reduced adipose inflammation and plasma and liver triglycerides without altering glucose homeostasis. It has also been reported that an SOD mimetic reduced plasma free fatty acids without altering glucose levels. Conversely, $SOD1^{-/-}$ mice exhibit impaired glucose homeostasis in normal diet-fed conditions, but not with high fat diet feeding. These results indicate that the effect of SOD1 in modulating glucose versus lipid metabolism will depend on the diet type.

Translational Significance

The lack of potent and highly bioavailable antioxidants is considered to be a challenge in antioxidant therapy. Our findings are relevant to consider Nano for the treatment of lipid disorders in obesity. Our findings are also relevant to understanding the mechanisms associated with the altered energy balance in ALS patients (who exhibit an increase in SOD activity). These ALS patients exhibit hypermetabolism and a high energy diet has been shown to improve patient survival. Our data show that Nano can promote both glucose and fatty acid metabolism. Since a high fat diet provides more energy, it may balance the energy-deficient state seen in ALS patients.

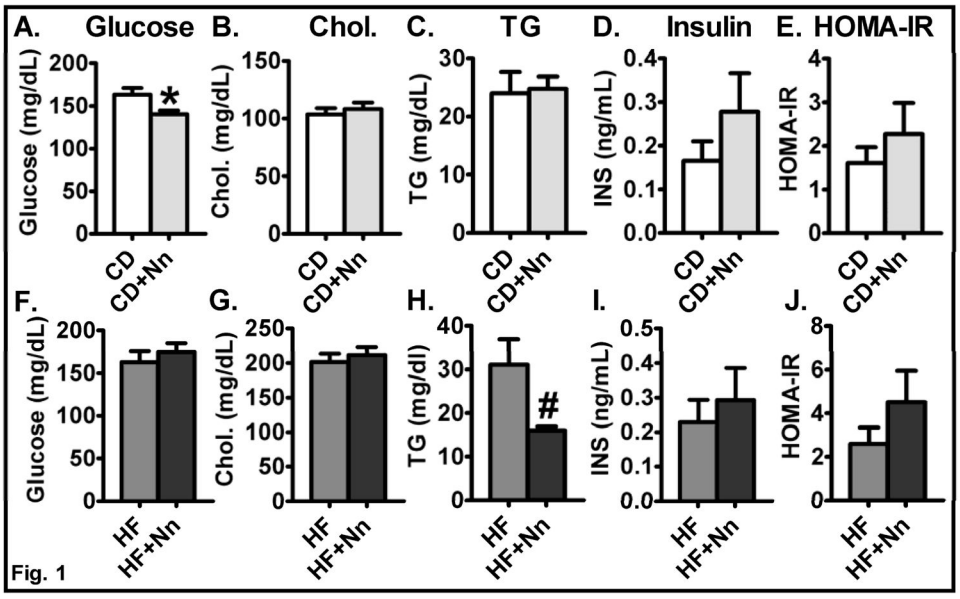

Fig. 1. Effect of Nano on metabolic variables

Fasting blood glucose (A, F), Serum total cholesterol (B, G), triglycerides (C, H) are shown. Values are expressed as mean ± SEM of 12–16 mice in each group. Insulin (D, I) and insulin resistance via HOMA IR (E, J) were recorded in CD and HF diet-fed mice. Values are expressed as mean ± SEM of 6–8 mice in each group. $^{*}P<0.05$ and $^{\#}P<0.01$ vs control. CD, chow diet; HF, high fat diet; and Nn, nanoSOD.

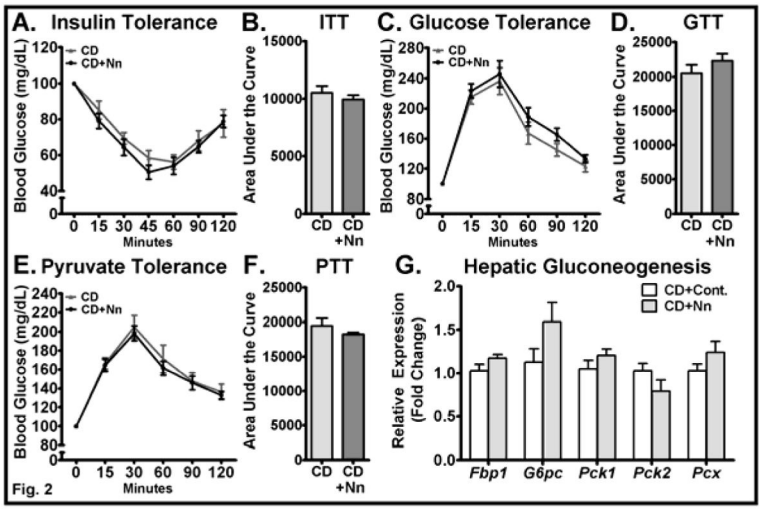

Fig. 2. Effect of Nano on systemic insulin sensitivity, glucose disposal, and hepatic glucose output

Mice were intraperitoneally injected with insulin for insulin tolerance test and blood glucose was recorded at indicated time points (A). Area under the curve glucose values from ITT were determined (B). GTT was performed by injecting an acute bolus of glucose and blood glucose was determined at various time points (C). Area under the curve glucose values from GTT were recorded (D). PTT was performed by injecting an acute bolus of sodium pyruvate and blood glucose was determined at various time points (E). Area under the curve glucose values from PTT were recorded (F). Blood glucose values for ITT, GTT, and PTT are plotted as percent change from baseline (0 min). Values are expressed as mean ± SEM of 6–8 mice in each group. Total RNA was extracted from liver and real-time PCR was carried out for genes involved in gluconeogenesis (G). Values are normalized to 18S RNA and are mean ± SEM of 6–8 samples per group. CD, Chow diet. HF, High fat, Nn, nanoSOD.

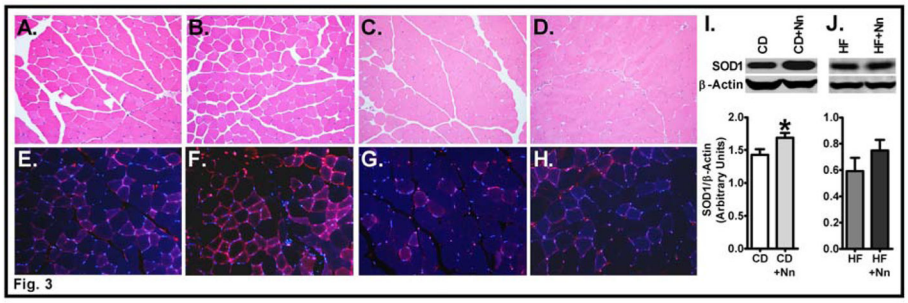

Fig. 3. Effect of Nano on markers of muscle histology and SOD1 content

Muscle sections were stained with hematoxylin and eosin for histological analysis. Photomicrographs (20X) from CD (A), CD+Nano (B), HF (C), and HF+Nano (D) are shown. Muscle sections were stained for SOD1 protein content and fluorescent images obtained at 20X magnification from CD (E), CD+Nano (F), HF (G), and HF+Nano (H) groups. Representative picture from 3 samples per group is shown. Western blot analysis of SOD1 protein in muscle from CD (I) and HF diet-fed mice (J) are shown. Bands were quantified and values normalized to β-actin. Values are expressed as mean ± SEM of 6–8 samples per group.* $P<0.05$ vs CD. CD, Chow diet. HF, High fat, Nn, nanoSOD.

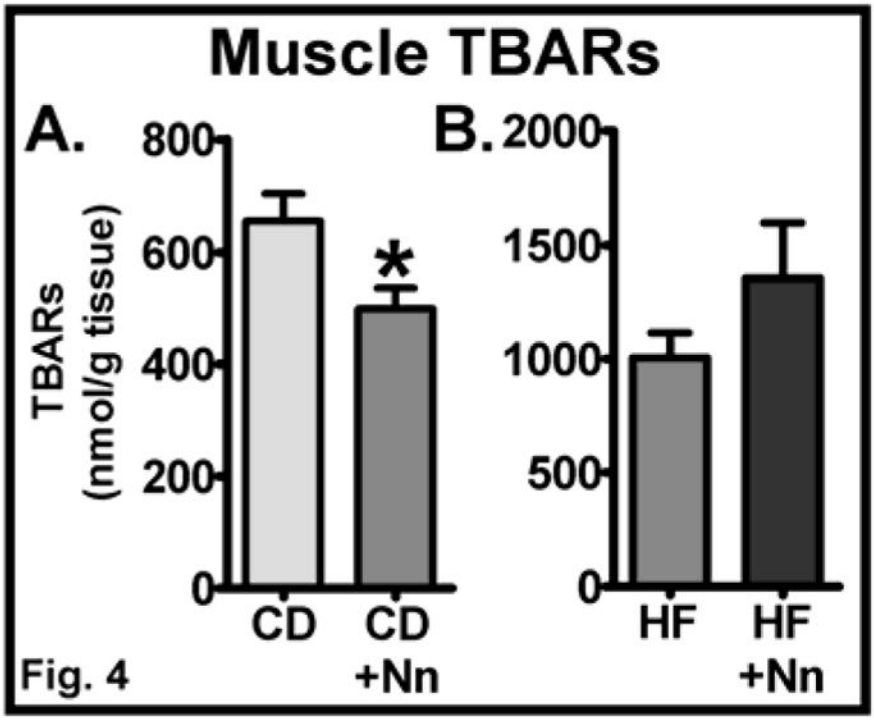

Fig. 4. Effect of Nano on skeletal muscle oxidative stress

The levels of TBARs, a marker of oxidative stress, were analyzed in skeletal muscle from CD (A) and HF diet-fed mice (B). Values are expressed as mean ± SEM of 5–8 samples/group. $^{*}P<0.05$ vs CD. CD, Chow diet. HF, High fat, Nn, nanoSOD.

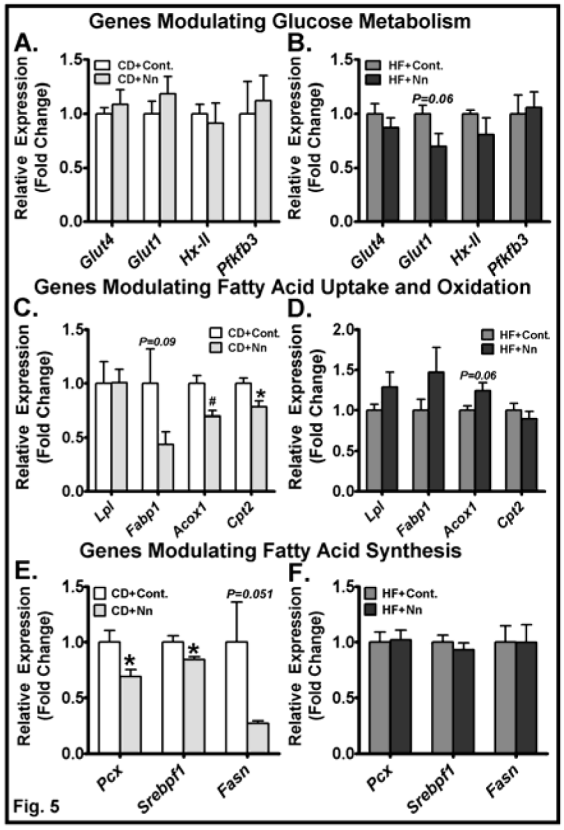

Fig. 5. Effect of Nano on muscle expression of genes involved in glucose and lipid metabolism

Total RNA was extracted from skeletal muscle and real-time PCR was carried out for genes involved in glucose metabolism (A, B), genes modulating fatty acid uptake and oxidation (C, D), and genes modulating fatty acid synthesis (E, F). Values are normalized to 18S RNA and are mean ± SEM of 6–16 samples per group. $^{*}P<0.05$ and $^{\#}P<0.01$ vs. CD. CD, Chow diet. HF, High fat, Nn, nanoSOD.

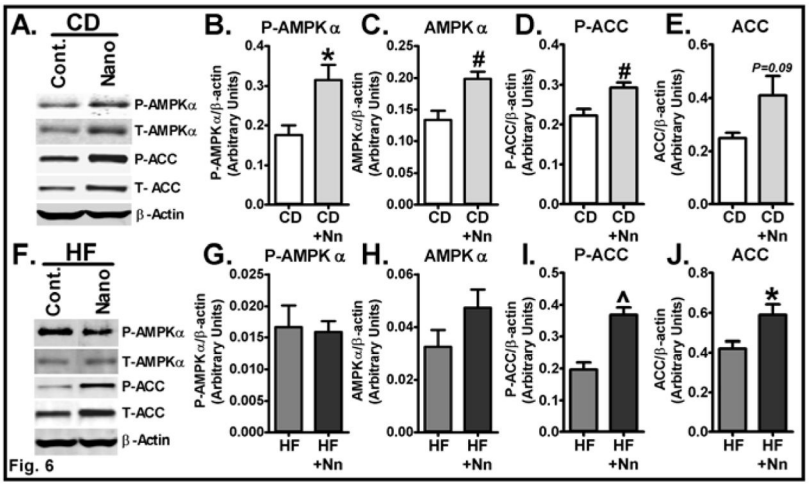

Fig. 6. Effect of Nano on markers of AMPK signaling in muscle

Muscle homogenates from CD and HF diet-fed mice treated with Nano were subjected to western blot analysis for markers of AMPK signaling. Representative band from each group in CD (A) and HF diet-fed (F) mice are shown. Bands were quantified and values normalized to β-actin. Protein levels of phospho-AMPKα (P-AMPKα), total AMPKα, phospho ACC (P-ACC), and total ACC from CD (B–E) and HF diet-fed mice (G–J) are shown. Values are expressed as mean ± SEM of 6–8 samples/group. *P<0.05, $^{\#}P$<0.01, and ^P<0.001 vs CD or HF controls. CD, Chow diet. HF, High fat, Nn, nanoSOD.

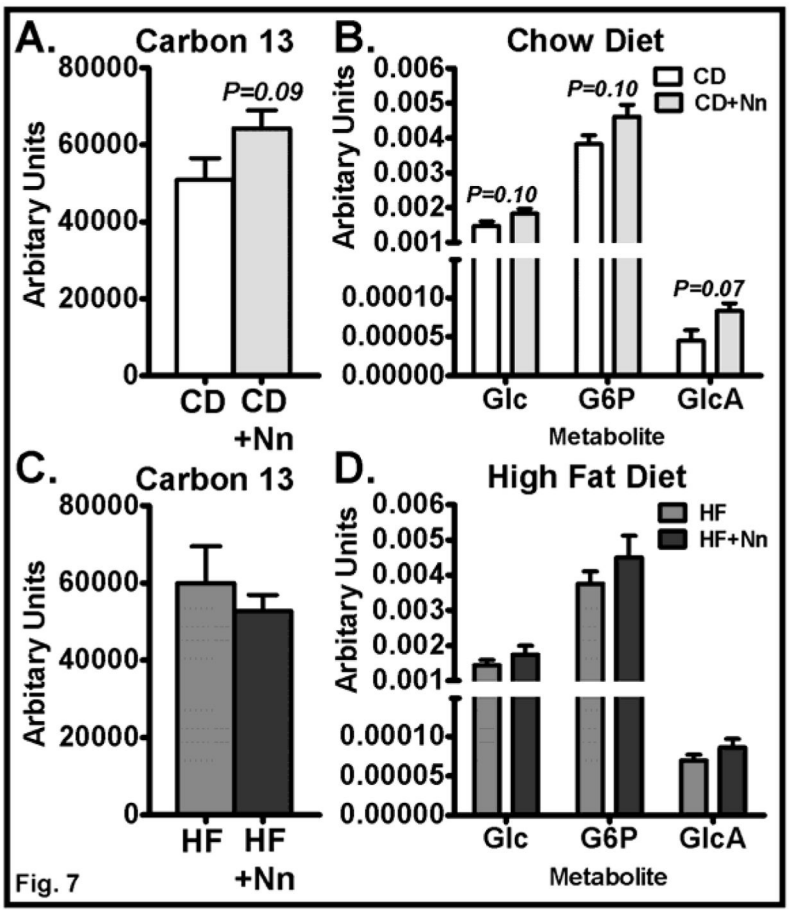

Fig. 7. Effect of Nano on ^{13}C enrichment in muscle metabolites

Targeted metabolomics analysis was performed to determine the ^{13}C enrichment in muscle metabolites. Control and Nano-treated mice were injected i.v. with stable isotope-labeled $^{13}C^{6}$ glucose and sacrificed after 15 min. of injection. ^{13}C enrichment of muscle metabolites and relative amounts of ^{13}C-labeled glucose, G6P, and glucuronic acid in CD (A, B) and HF-fed mice (C, D). Values are mean ± SEM of 6–8 samples/group. CD, Chow diet. HF, High fat, Nn, nanoSOD, G6P, glucose-6 phosphate, GlcA, glucuronic acid. The bar graph in (A) is labeled with Student's *t* pairwise *P* values and (B) is labeled with Benjamini-Hochberg corrected *P* values.

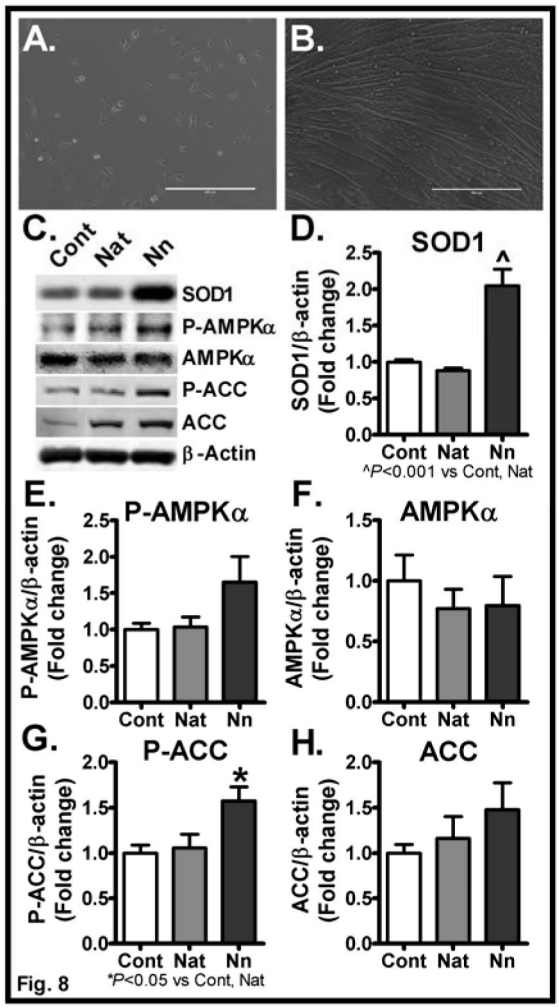

Fig. 8. Effect of Nano in altering AMPKα signaling in C2C12 differentiated myotubes

Micrographs (10X) of un-differentiated myoblasts (A) and differentiated myotubes at Day 7 (B) are shown. Myotubes were treated with native SOD or Nano for 6 h. Cells were rinsed and incubated in fresh growth media overnight. Cell lysates were analyzed for SOD1 uptake and markers of AMPK signaling. Representative bands were shown (C). Band intensities were quantified and normalized to β-actin (D–H). Values are expressed as mean ± SEM of 3 independent experiments. *P* values were determined using the 1-way ANOVA followed by Tukey's multiple comparison test. Cont, Control, Nat, Native, and Nn, nanoSOD.

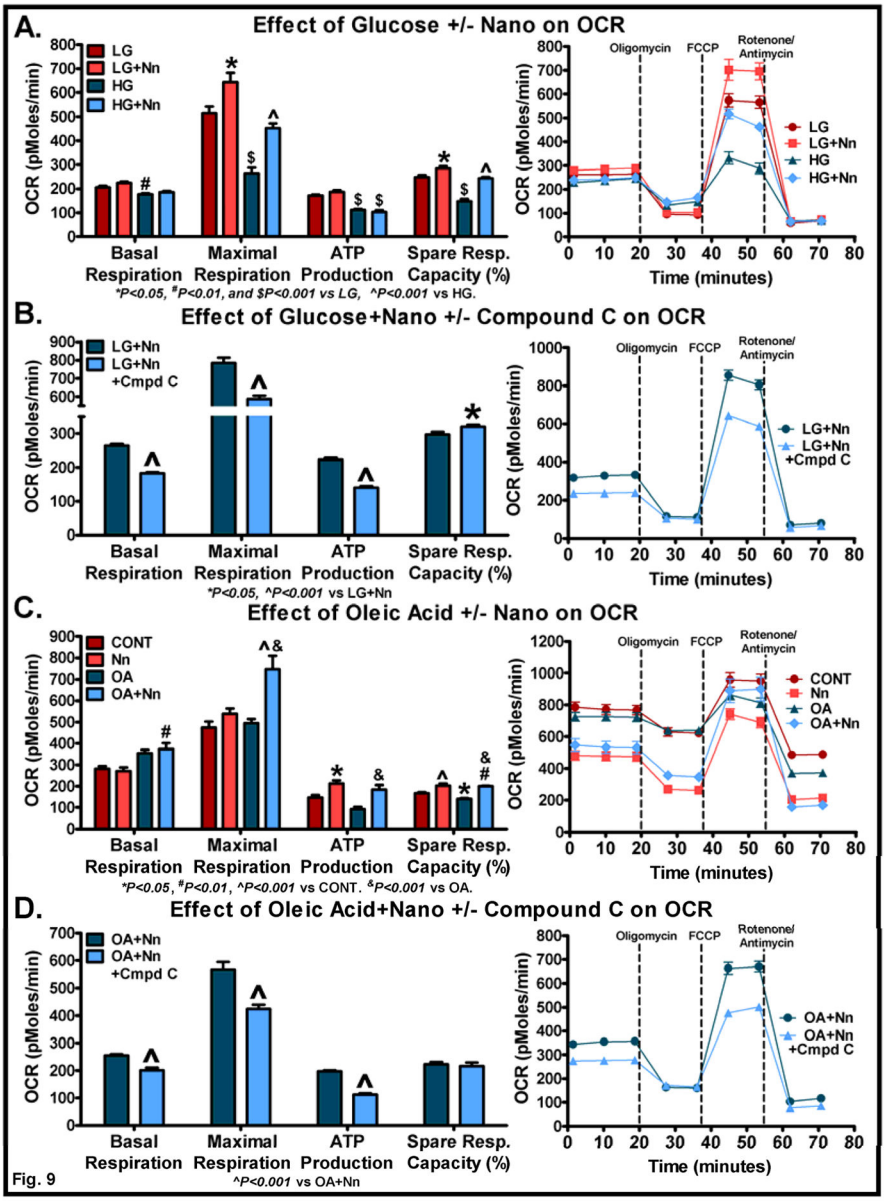

Fig. 9. Effect of Nano in altering mitochondrial respiration in the presence of glucose or fatty acid

C2C12 myoblasts were pre-treated with Nano (200 units/mL) for 6 h. The cells were washed and incubated overnight in fresh growth media. The following day, cells were washed and supplemented with XF assay medium containing low (2.5 mM) or high glucose (25 mM). OCR was determined as described in Methods. The effect of glucose in the presence or absence of Nano on basal respiration, maximal respiration, ATP production, and spare respiratory capacity (%) are shown (A). Cells were pre-treated with Compound C for 1 h followed by treatment with Nano for 6 h. Cells were washed and incubated with fresh medium overnight in the presence or absence of Compound C in respective groups. The following day, cells were washed and supplemented with XF assay medium containing 2.5 mM glucose with or without Compound C. OCR was determined as described above (B).

C2C12 cells pretreated with Nano the previous day were supplemented with XF assay medium in the presence of oleic acid (90 μM) and OCR determined (C). Cells were pre-treated with Compound C and/or Nano as described above. The following day, cells were supplemented with XF assay medium containing 60 μM oleic acid with or without Compound C and, OCR was determined as described above (D). The actual trace and sequence of additions used to calculate OCR are shown in each panel (A–D). Basal respiration: [(last rate measurement before oligomycin injection) – Non-mitochondrial respiration (minimum rate measurement after rotenone/antimycin injection)]; Maximal respiration: [(maximum rate measurement after FCCP injection) – Non-mitochondrial respiration (minimum rate measurement after rotenone/antimycin injection)]; ATP production: [(last rate measurement before oligomycin injection) – (minimum rate measurement after oligomycin injection)]; Spare respiratory capacity (%): [(maximal respiration)/(basal respiration) x 100]. Values are mean ± SEM of 10 samples/group. *P* values were determined using the 1-way ANOVA followed by Tukey's multiple comparison test. For experiments with 2 groups (B & D), Student's *t*-test was performed.